Local measurements of tearing mode flows and the magnetohydrodynamic dynamo in the Madison Symmetric Torus reversed-field pinch

D. A. Ennis,[1,2] D. Craig,[3] S. Gangadhara,[1,2] J. K. Anderson,[1] D. J. Den Hartog,[1,2] F. Ebrahimi,[1,2] G. Fiksel,[1,2] and S. C. Prager[1,2]
[1]*The University of Wisconsin-Madison, Madison, Wisconsin 53706-1390, USA*
[2]*Center for Magnetic Self-Organization in Laboratory and Astrophysical Plasmas, Madison, Wisconsin 53706-1390, USA*
[3]*Wheaton College, Wheaton, Illinois 60187-5501, USA*

(Received 28 January 2010; accepted 4 June 2010; published online 11 August 2010)

The first localized measurements of tearing mode flows in the core of a hot plasma are presented using nonperturbing measurements of the impurity ion flow. Emission from charge exchange recombination is collected by a novel high optical throughput duo spectrometer providing localized (± 1 cm) measurements of C^{+6} impurity ion velocities resolved to <500 m/s with high bandwidth (100 kHz). Poloidal tearing mode flows in the Madison Symmetric Torus reversed-field pinch are observed to be localized to the mode resonant surface with a radial extent much broader than predicted by linear magnetohydrodynamic (MHD) theory but comparable to the magnetic island width. The relative poloidal flow amplitudes among the dominant core modes do not reflect the proportions of the magnetic amplitudes. The largest correlated flows are associated with modes having smaller magnetic amplitudes resonant near the midradius. The MHD dynamo due to these flows on the magnetic axis is measured to be adequate to balance the mean Ohm's law during reduced tearing activity and is significant but does not exclude other dynamo mechanisms from contributing during a surge in reconnection activity. © *2010 American Institute of Physics*.
[doi:10.1063/1.3458667]

I. INTRODUCTION

The linear theory of resistive tearing modes, and more specifically the resulting fluctuations in the magnetic and flow fields, are well established.[1] Additionally, study of the magnetic fields of tearing modes in nonlinear systems is widespread.[2] On the contrary, flows due to tearing modes are not a well understood feature in the nonlinear regime. Nonlinear analytical predictions of the flow have been derived for the case of a single dominant mode referred to as the "Rutherford regime," which is relevant to the tokamak configuration.[3,4] Nevertheless, previous experimental results demonstrate the importance of fully nonlinear effects such as tearing mode saturation and coupling.[5,6] In nonlinear magnetohydrodynamic (MHD) computations, numeric parameters such as viscosity and pressure often alter the generated flow structure much more than the magnetic dynamics. Flows associated with tearing modes have previously been inferred from $\mathbf{E}\times\mathbf{B}$ measurements,[7] observed in the plasma edge with a spectroscopic probe,[8] and measured in the core with line-integrated spectroscopy.[9,10] Yet, direct experimental measurement of the spatial structure of tearing mode flows in the core of a hot plasma has not been achieved previously. A more complete understanding of the tearing mode instability in the nonlinear regime requires an improved account of the associated flow fluctuations.

The presence of tearing mode flows has a number of potential consequences in both laboratory and astrophysical plasmas, including viscous ion heating, particle, momentum and energy transport. Furthermore, local fluctuations resulting from tearing modes are known to play a significant role in establishing the equilibrium plasma through dynamo action. For example, the MHD dynamo is the constructive interference of velocity and magnetic fluctuations with the effect of relaxing the current profile in laboratory configurations such as the reversed-field pinch[11] (RFP) and the spheromak.[12] Dynamo action has been measured to be significant in both the edge[7,8] and core[9,10,13] of the RFP, yet the understanding of the dynamo spatial structure in the core remains incomplete.

The first localized measurements of flow structures resulting from resistive tearing mode instabilities in the core of a hot plasma are made possible by a novel charge exchange recombination spectroscopy (CHERS) diagnostic. The CHERS diagnostic technique[14] is routinely employed for localized equilibrium values of ion velocity and temperature on many plasma devices[15] including the Madison Symmetric Torus (MST).[16,17] However, measurements using CHERS with high enough bandwidth to resolve fluctuations in velocity due to tearing modes were reported only once[18] and a correlation with tearing modes was not performed.[19] The construction of a new optical spectrometer with simultaneously high throughput and large dispersion provides flow measurements localized to ± 1 cm with 100 kHz bandwidth yielding the spatial structure of tearing mode flows.

The remainder of this article details the measurement of tearing mode flow profiles in the core of MST and their contributions to the MHD dynamo. Section II begins by describing the unique CHERS diagnostic deployed on MST with particular attention to a custom-built spectrometer allowing for fast localized measurements of ion parameters. Magnetic measurements and correlation methods used to dis-

cern velocity fluctuations associated with individual tearing modes resonant in the plasma core are also explained. Measurements of tearing mode flow profiles are presented in Sec. III for plasmas with three different magnetic mode spectra. Poloidal tearing mode flows in MST are observed to be localized to the mode resonant surface with a radial extent much broader than predicted by linear MHD theory but comparable to the magnetic island width. The relative poloidal flow amplitudes among the dominant core modes do not reflect the proportions of the magnetic amplitudes. During modest tearing activity, the largest correlated flows are associated with modes having smaller magnetic amplitudes resonant near the midradius. Periods of intense reconnection activity demonstrate a substantial increase and broadening of correlated flow profiles. Measurements in plasmas with a single mode dominating the magnetic spectrum demonstrate a broadening of the dominant mode flow structure consistent with an increase of the magnetic island width but yielding a hollow poloidal flow profile. In Sec. IV, the total MHD dynamo on the magnetic axis is determined from the tearing mode flows along with contributions to the total MHD dynamo off-axis. The measured MHD dynamo on the magnetic axis is adequate to balance the mean Ohm's law during reduced tearing activity and is significant but does not exclude other dynamo mechanisms from contributing during a surge in reconnection activity.

II. MEASUREMENT TECHNIQUE

A. Fast localized flow measurements

Measurements of ion parameters in the core of MST have previously been attained using ion Doppler spectroscopy.[20,21] Ion flows are established along a line of sight by the observed Doppler shift of a radiated line spectrum. However, line-integrated techniques are especially problematic for plasma fluctuations, which are often spatially localized and can be muted or canceled along a line of sight. The CHERS approach incorporates a high energy neutral particle source with Doppler spectroscopy to further stimulate emission and provide localized flow measurements at the intersection of the neutral particle beam and the optical line of sight. A long pulse (20 ms) diagnostic neutral beam injects neutral hydrogen atoms radially across MST with an average energy of 49 keV. The absorbed diagnostic neutral beam power is on the order of 100 kW, while the total plasma power is ~ 3 MW and on that account the beam does little to alter the plasma behavior. An array of eleven portholes spanning the MST minor diameter is oriented such that sightlines through these ports are perpendicular to the beam trajectory, providing measurements of velocity along the lines of sight. The viewing array affords ten poloidal velocity measurements in addition to a single radial velocity measurement at $\rho/a \approx 0$ supplied by the central sightline passing through the magnetic axis (see Fig. 1). Measurements presented range from $0.00 \leq \rho/a \leq 0.75$ as charge exchange radiation in the cooler edge of the plasma is small.

A custom-built duo spectrometer has been constructed[22] with high optical throughput (transmission efficiency of 6% and etendue of 0.80 mm^2 sr divided into two simultaneous measurements) and good wavelength resolution ($\lambda/\Delta\lambda = 5600$). The spectrometer is optimized for the 343.4 nm C VI spectral line corresponding to the $n=7$ to $n=6$ transition of C^{+5} due to its bright intensity in MST and isolation from other contaminating emission. While limited by the total number of photons emitted by the driven charge exchange process, the 10 μs temporal resolution of the spectrometer is fast enough to resolve flow fluctuations associated with tearing modes and ion heating due to reconnection in MST.

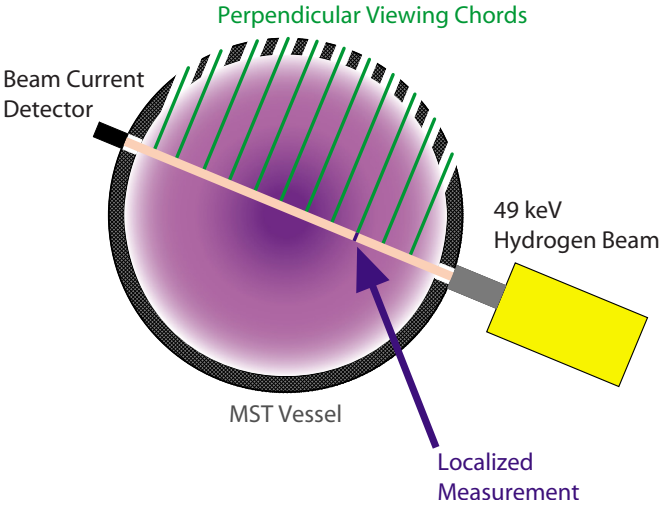

FIG. 1. (Color online) Poloidal cross section of MST showing the beam path and viewing chords available for CHERS measurements.

Precise quantification of the electron-impact excitation observed from each viewing port is essential in MST because the line-integrated electron-impact emission is often significantly larger than the charge exchange radiation induced by the neutral beam. Consequently, a duo spectrometer with two independent views was developed to simultaneously distinguish the localized charge exchange emission from the background electron-impact excitation. Both optical views of the duo spectrometer are coupled to the plasma by 3.0 m long fiber bundles. The two fiber bundles are designed to share a viewing port on MST at the same impact parameter. The fiber bundles are toroidally displaced from each other such that one fiber bundle views the beam directly, measuring both the background electron-impact excitation and the charge exchange driven emission, while the second fiber bundle only collects background emission from electron-impact excitation (Fig. 2). Measurements of C^{+6} ion properties are localized to a 2 cm radial extent corresponding to the intersection volume of the diagnostic neutral beam path and the light cone of the fiber bundle view. Nonetheless, the radial measurement spacing of the poloidal profile shown in Fig. 1 is constrained by the locations of the MST portholes spaced about 9 cm apart.

The process of calculating impurity ion parameters from the spectrometer wavelength channels is accomplished by an algorithm of iterative minimizations to the deviation of an atomic model from the measured data.[23] The emission model includes line splitting due to spin-orbit coupling (fine structure) and O VI contamination. Models for both the back-

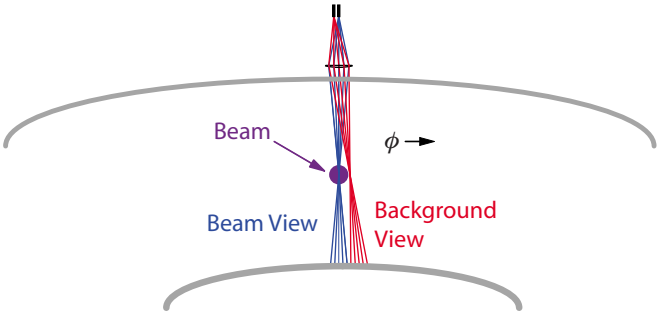

FIG. 2. (Color online) Radial view along the diagnostic neutral beam path emphasizing the toroidal displacement of the background spectroscopic view essential for localized measurements.

ground electron-impact and charge exchange driven emission have been created using the Atomic Data and Analysis Structure (ADAS) database.[24] Additionally, the impurity ions measured by the CHERS diagnostic are assumed to be a good proxy for the bulk ion motion, which is the case in single-fluid MHD analysis where perpendicular flows are governed by $\mathbf{E}\times\mathbf{B}$ forces.

Fluctuation quantities measured by the CHERS diagnostic are ensemble averaged to reduce measurement noise. Furthermore, ion velocity power spectra are computed from each ensemble. The power spectrum of the impurity ion poloidal velocity measured by the CHERS diagnostic at the $\rho/a=0.55$ outboard viewing chord presented in Fig. 3 largely consists of measurement noise; however, correlation with the magnetic mode amplitudes extracts the part that is due to tearing modes. The velocity power spectrum is broadband, with a spike at low frequencies likely due to secular changes in the plasma on slow timescales. In the frequency range of the $m=1$ magnetic mode activity in MST, the velocity power spectrum is generally flat with a bump between 10 and 20 kHz foreshadowing significant coherence between the velocity fluctuations at $\rho/a=0.55$ and the tearing mode magnetic amplitude.

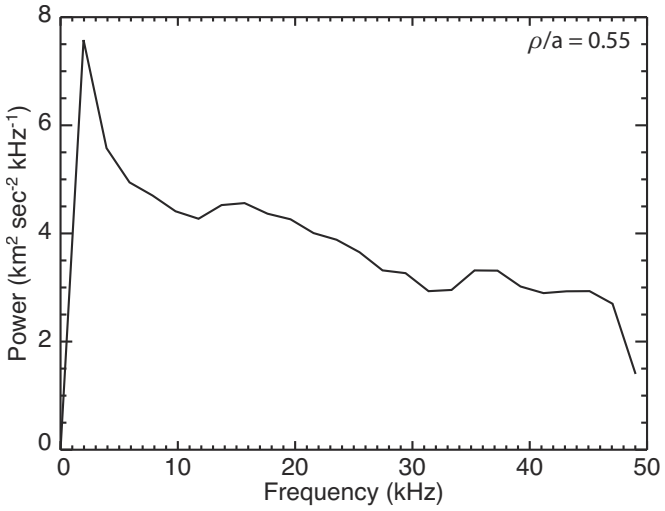

FIG. 3. Poloidal velocity power spectrum for the $\rho/a=0.55$ outboard CHERS measurement location.

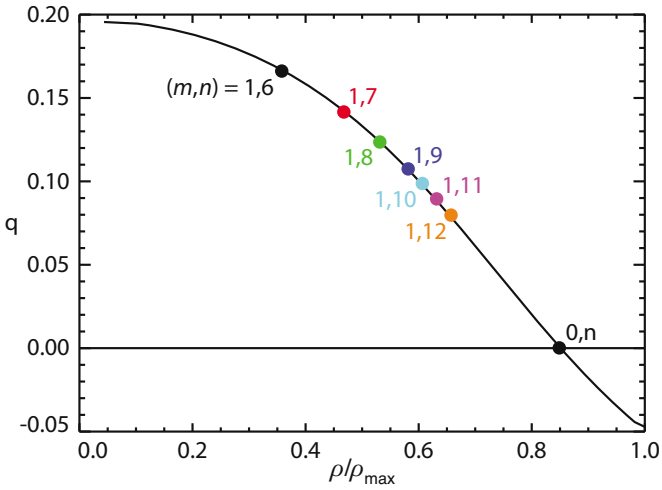

FIG. 4. (Color online) Typical safety factor profile in MST during quiescent plasma periods with the resonance surfaces of the dominant modes highlighted.

B. Extracting tearing mode flows

The CHERS diagnostic yields ion velocity as a function of time at a single spatial point. Velocity measurements are comprised of tearing mode flows, other flows and noise (Fig. 3). Extraction of the flows due only to tearing modes is accomplished through a correlation analysis of the measured velocity and magnetic measurements from a toroidal array of coils. The magnetic signals are well resolved; thus, a correlation removes uncorrelated flow and noise. Furthermore, a correlation with magnetic signals supplies mode-resolved tearing flows because the correlation analysis is performed with individual mode numbers. Finally, ensemble averaging over many similar plasmas further combats the high noise levels in individual plasma discharges. Details of the correlation analysis and the ensemble averaging will be explained in this section.

The RFP magnetic structure is highly sheared, resulting in a reversal of the toroidal magnetic field from the core to the edge of the plasma.[25,26] The RFP safety factor (ratio of the magnetic field transits in the toroidal direction to transits in the poloidal direction) is a monotonically decreasing function of radius. Inspection of the MST safety factor profile (Fig. 4) reveals many tearing mode resonances across the plasma radius where the mode wavevector is perpendicular to the mean magnetic field ($\mathbf{k}\cdot\mathbf{B}=0$). Dominant modes resonant in the core of the RFP have a poloidal mode number, $m=1$, and a toroidal mode number, $n\geq 2R/a$. In general, the largest magnetic mode in the core of MST is characterized by $m=1$, $n=6$, while modes of higher n number decrease in amplitude considerably as a function of n. All $m=0$ magnetic modes are resonant at the reversal surface but are not observed to be large in the core. Magnetic fluctuations play a substantial role in the global dynamics of the RFP and much work has been carried out previously to characterize magnetic tearing mode behavior in the RFP.[5,27–33]

Direct measurements of the tearing mode spectrum in the core of MST are not available for any quantity, including magnetic fields. Nevertheless, magnetic mode spectral mea-

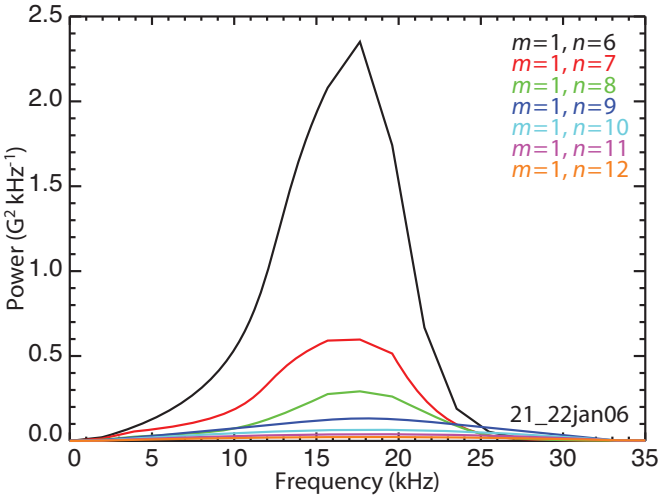

FIG. 5. (Color) Magnetic mode power spectra of the poloidal field measured at the edge of the plasma for the dominant $m=1$ modes in MST during quiescent periods.

surements are routinely made at the plasma wall by arrays of magnetic coils. Concurrent measurements at 64 toroidal locations evenly distributed around the toroidal circumference permit a spatial Fourier decomposition of the magnetic signals into discrete n mode constituents. Ensembles of the $m=1$ tearing mode magnetic amplitudes measured by the toroidal array during quiescent plasma periods yield the power spectra plotted in Fig. 5. In MST, $m=1$ magnetic mode activity is generally peaked between 10 and 20 kHz with the total power of each mode resonant in the plasma dropping sharply with higher toroidal mode number. A small shift of the mode power centroid to higher frequency is also evident with increasing toroidal mode number, as expected if the modes have similar toroidal phase velocities in the laboratory frame. Modes with a toroidal mode number above $n=12$ continue to decrease in power and are approximately two orders of magnitude smaller in total power than the dominant $n=6$ mode.

Tearing mode magnetic fluctuations in the plasma core are inferred from the edge array of coils as the dominant $m=1$ core magnetic mode structures are understood to be global and coherent across the entire plasma radius. For the present analysis, experimental and computational data are combined to provide the best estimate of the absolute magnitude and phase of the dominant modes at all radial locations in the plasma core. Predictions for the spatial structure of the magnetic mode amplitudes provided by DEBS, a nonlinear single-fluid MHD computation code,[34] are scaled to match the amplitudes of line-integrated measurements from a Faraday rotation diagnostic.[35] The inferred relations between the magnetic dynamics at the wall and in the core used in this work are in agreement with prior experimental results in the RFP and predictions by MHD computational modeling.[26,30] The multitude of tearing modes resonant in MST are responsible for small levels of continual reconnection throughout the plasma discharge as evidenced by the finite amplitude of the largest tearing mode measured at the vessel wall (Fig. 6). Periodically an impulsive surge in the reconnection activity is observed on a fast timescale (~ 100 μs) which is not externally imposed. The surge in reconnection occurs for all tearing modes resonant in the experiment, which generates multiple reconnection sites simultaneously across the plasma volume and is referred to as a "sawtooth crash."[36] Additionally, fluctuation levels of almost all plasma parameters are many times larger during a sawtooth crash. For the purposes of this work, plasma discharges are segmented into two distinct types of intervals. Quasiequilibrium periods, defined to be at least 1.0 ms away from any sawtooth crash, are referred to as "quiescent periods" during which fluctuation levels are relatively low. Quiescent periods are subdivided into time windows of

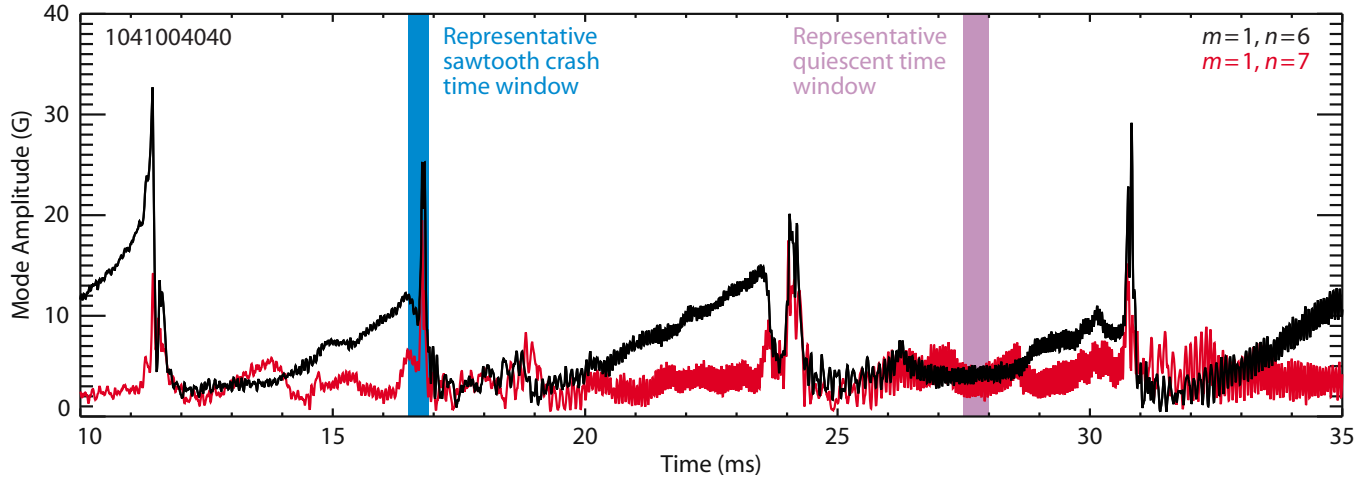

FIG. 6. (Color online) Poloidal magnetic mode amplitudes for the two largest modes in MST measured by the toroidal array at the plasma wall. Sawtooth crashes are clearly evident at 11.5, 16.8, 24.1, and 30.8 ms during the discharge window. A time window from −0.3 to +0.1 ms relative to the sawtooth crash at 16.8 ms is shown, representing a single sawtooth interval included in the ensemble analysis. Likewise, a 0.5 ms window indicating one quiescent interval is highlighted during a period of low magnetic fluctuations. As many as three sawtooth events and twenty-five quiescent intervals per plasma discharge routinely were included in the ensembles.

0.5 ms to capture at least five complete oscillations of the MHD resistive tearing modes. The second type of interval was constructed around sawtooth crash events, providing measurements during varying amounts of reconnection. Sawtooth crash ensembles were created with 0.4 ms windows selected from −0.3 to +0.1 ms with respect to the sawtooth crash. The reduction of the time window duration to 0.4 ms is an attempt to capture the fast dynamics taking place at the crash while still affording sufficient time to resolve a few complete cycles of the tearing modes necessary for the Fourier analysis. The asymmetric window relative to the crash was necessary to avoid periods of no plasma rotation often occurring and persisting after a sawtooth crash. Figure 6 illustrates the selection of a single quiescent interval and sawtooth event.

The low signal to noise ratio of the CHERS flow measurement makes ensemble averaging essential to reduce noise and discern significant plasma behavior. An ensemble of many time windows is also an average over toroidal and poloidal angle in the MST geometry, commonly referred to as a flux surface average. During ensemble selection, many consecutive quiescent windows or sawtooth crash events are chosen if they meet constraints on plasma parameters such as: electron density (n_e), plasma current (I_p), and reversal parameter ($F \equiv \mathbf{B}_\phi(a)/\langle \mathbf{B}_\phi \rangle_{vol}$). All data presented herein are characterized by $n_e \sim 1.0 \times 10^{13}$ cm^3, $I_p \sim 400$ kA and $F \sim -0.23$.

The fluctuating flow associated with each tearing mode is described by

$$\mathcal{V}_n = \frac{|\tilde{v}||\tilde{b}_n|\gamma_{b_n v}}{\sqrt{|\tilde{b}_n|^2}}, \tag{1}$$

where $\tilde{v}$ represents the total measured fluctuating velocity, $\tilde{b}_n$ the fluctuating magnetic amplitude of the mode, and $\gamma_{b_n v}$ the coherence between the two signals. The coherence baseline of the tearing mode flow measurement is well characterized by the magnitude of coherence between two random (uncorrelated) signals

$$\gamma_{b_n v}^{\text{baseline}} = \frac{1}{\sqrt{N_{\text{event}}}}, \tag{2}$$

where N_{event} is the number of events in the ensemble. Any measured coherence greater than the coherence baseline is considered to be significant. Therefore, larger ensembles reduce the minimum correlated flow that can be resolved.

The method of extracting tearing mode flows does have several limitations. First, a measurement at a single spatial location does not supply tearing mode flows at every instant in time; instead, it yields an ensemble averaged flow. Second, tearing modes must be rotating and not locked to the laboratory frame during all ensemble windows to ensure a random sample of the mode in space or phase. Locking can be a frequent occurrence in MST, especially during high current ($\geq$400 kA) discharges. Lastly, the method is limited to only extracting flows due to tearing modes, not flows from any other source.

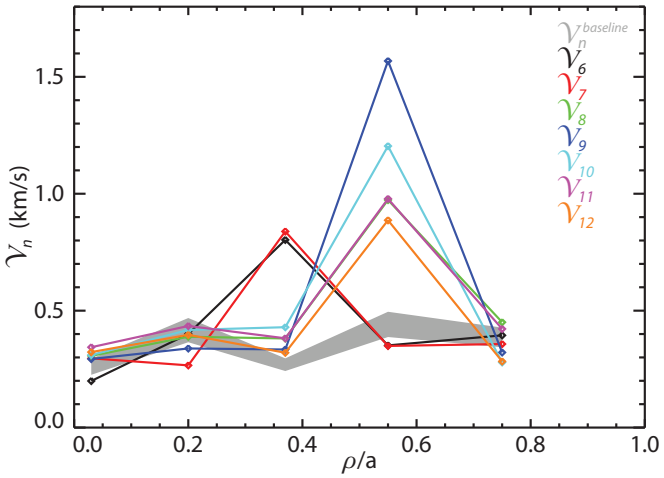

FIG. 7. (Color) The poloidal velocity pseudo n-spectrum of the impurity ions measured by the CHERS diagnostics at the five outboard radial locations during quiescent periods. Peaks of the correlated flow associated with each tearing mode are well matched to the radial location of the mode resonant surfaces.

III. TEARING MODE FLOWS

A. Quiescent periods

The impurity ion velocity pseudo n-spectrum denoted by $\mathcal{V}_n$ is calculated according to Eq. (1) and determines the magnitude of the fluctuating velocity in the poloidal direction that is correlated with each tearing mode. The gray band represents the velocity pseudo n-spectrum baseline for $\sim$1000 quiescent windows and is defined by the combination of Eqs. (1) and (2). The seven different baselines corresponding to each of the modes included in Fig. 7 have been combined into the gray band, illustrating the spread of the seven velocity pseudo n-spectrum baselines. The largest correlated velocities are observed near the midradius with the $n=9$ and $n=10$ toroidal modes, while modest flows are associated with the dominant $n=6$ mode. Poloidal tearing mode flow amplitudes during quiescent intervals are measured to be approximately three orders of magnitude less than the Alfvén velocity ($v_A \equiv B/\sqrt{\mu_0 \rho}$) of $\sim 2.0 \times 10^3$ km/s. Furthermore, very little correlated flow exists at the center of the plasma or the maximum radial extent of the measurement.

The structure of the poloidal tearing mode flows exhibits three principle features: (a) the flow due to each mode is peaked near the radius of its resonant surface, (b) the radial extent of the correlated flows are consistent with the expected island sizes, and (c) the relative flow amplitudes are dissimilar from the magnetic n-spectrum. Strong agreement exists between the radial position of the correlated flow peaks and the mode resonant surfaces highlighted on the safety factor profile in Fig. 4. Localization of the correlated flows near the mode resonant surfaces, where reconnection occurs, suggests the measured flows are associated with reconnection on these surfaces. All tearing modes demonstrate significant correlated flow at a minimum of one measurement location with most modes having substantial correlated flow at only one measurement location. Therefore, we conclude that the radial extent of the flow fluctuations due to a

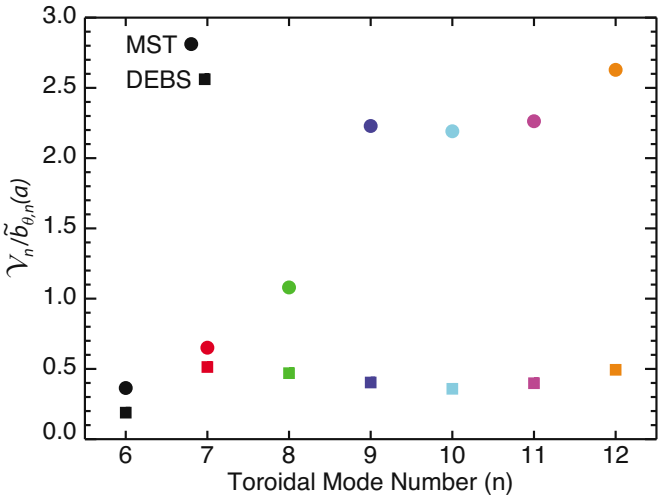

FIG. 8. (Color online) The ratio of the peak poloidal tearing mode flow to poloidal magnetic amplitude at the wall for each core mode measured in MST during quiescent periods (circles) and the corresponding multimode nonlinear DEBS calculations (squares). In each case, correlated velocity fluctuations are normalized to the Alfvén velocity and magnetic mode amplitudes are normalized to the mean magnetic field on-axis.

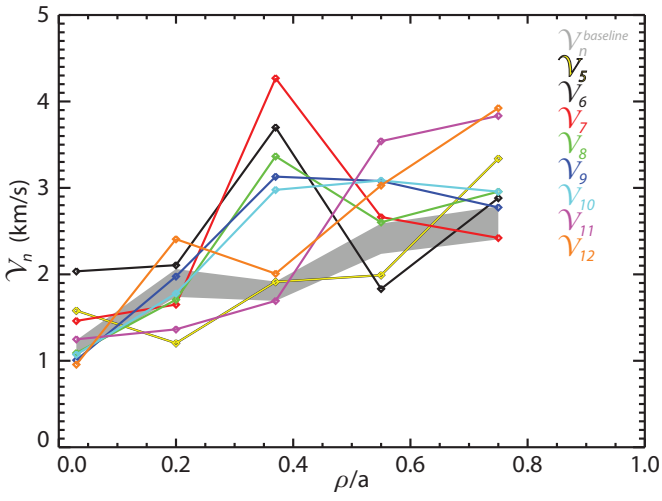

FIG. 9. (Color) The poloidal velocity pseudo n-spectrum of the impurity ions measured by the CHERS diagnostics at the five outboard radial locations during a sawtooth crash (−0.3 to +0.1 ms). Tearing mode flows during the crash are both large in amplitude and broad in radius but exhibit similar peak magnitudes.

single tearing mode is of the order of the CHERS measurement spacing (~9 cm). While a 9 cm spatial extent of the fluctuating velocity is narrow relative to the magnetic mode profiles, the flow structures are broad when compared to linear calculations where flow gradients are on the scale of the resistive layer width (~1 mm in MST). The measurements indicate that nonlinear contributions to the flow profile are important. Previous calculations of the tearing mode island width during quiescent periods estimate the dominant $n=6$ island width to be ~18 cm with the remaining $n=7$ to 12 islands having widths between 9 and 4 cm wide.[37] These island width calculations are mostly in agreement with the tearing mode flow profiles, perhaps suggesting that the radial extent of the tearing mode flow is related to the island width as a result of kinetic processes. It is also possible the radial flow profile is related to nonlinear MHD effects such as mode coupling or non-MHD physics. For example, a two-fluid analysis in MST yields an ion-sound gyroradius, $\rho_s \sim 1$ cm. While it is clear that a linear MHD description cannot explain the structure of the measured tearing mode flows, we are unable to distinguish which nonlinear effect is responsible for the broadening.

A prominent feature of the poloidal tearing mode flow spectrum is that the relative flow amplitudes do not resemble the poloidal magnetic spectrum which decreases monotonically from $n=6$ to higher toroidal mode numbers. Modest flows are observed near the axis of MST with the greatest flows at the midradius of the plasma, despite the dominant tearing modes being resonant closer to the axis. In contrast, predictions of the poloidal tearing mode flow n-spectrum using DEBS, a single-fluid MHD analysis in a cylindrical geometry, generally reflect the magnetic amplitude n-spectrum. A comparison of normalized tearing mode flows reveals that while the approximate magnitude of the flow velocities predicted by DEBS may be reasonable, the trend versus n mode number does not agree with the measurement (Fig. 8). Thus, it is likely that the total (radial, poloidal, and toroidal) tearing mode flow n-spectrum is very different from the magnetic mode n-spectrum. Then again, the difference between the measured flow and magnetic n-spectra could result from only sampling the poloidal component of the velocity. Due to the structure of the mean magnetic geometry in MST, poloidal CHERS measurements would be very sensitive to large parallel flows in the edge region where the mean magnetic field is nearly aligned with the poloidal direction. A toroidal CHERS view currently is being developed to investigate this detail further.

B. Impulsive reconnection

Measurements of tearing mode flows also have been made during intervals of intense fluctuations referred to as a sawtooth crash. A surge in reconnection during a sawtooth crash takes place at multiple tearing mode resonant surfaces across the plasma radius and is expected to drive large flows. Background electron-impact excitation emission increases dramatically during the sawtooth crash, reducing the signal to noise ratio of the charge exchange measurement. On the other hand, magnetic mode amplitudes grow substantially leading up to the crash, in turn driving strong flows and thereby making it possible to resolve the correlated flow spectrum despite the high background emission. Sawtooth crash ensembles have been generated using the same discharges and similar plasma parameters as the quiescent case.

Velocity fluctuation profiles measured during the sawtooth crash, plotted in Fig. 9, exhibit large flows correlated with tearing modes and are consistent with an increase of magnetic mode activity. In addition, most of the modes display a broader spatial structure denoted by significant correlated flow above the baseline at more than one measurement location. Broadening of the tearing mode flows is beyond what can be explained by movement of the resonance surfaces during a sawtooth crash. Yet, the tearing mode flows

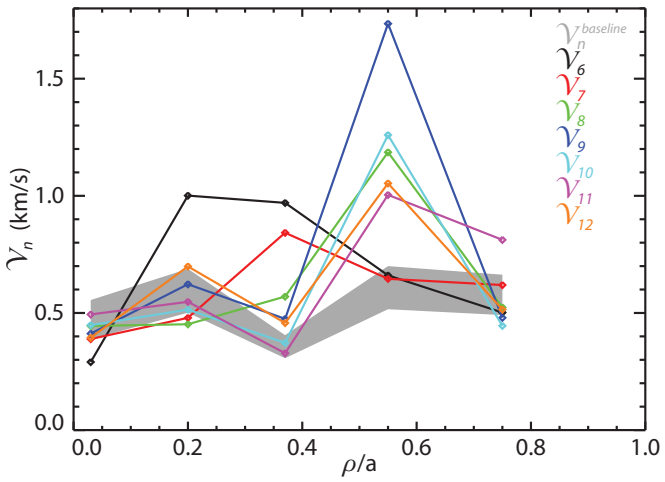

FIG. 10. (Color) The poloidal velocity pseudo n-spectrum of the impurity ions measured at the five outboard radial locations during QSH plasma periods.

generally remain peaked near the expected locations of the associated resonant surfaces. Interestingly, flows due to the different tearing modes have similar peak magnitudes, in contrast to the quiescent case where smaller magnetic mode amplitudes correspond to larger correlated poloidal flows. As a result, the flow n-spectrum better resembles the magnetic n-spectrum during a sawtooth crash. Finally, flow fluctuations near the magnetic axis are significantly correlated with the $n=5$ to 7 modes, contrary to the quiescent ensemble in which correlated flow magnitudes are measured to be similar to the baselines. Higher velocity pseudo n-spectrum baselines reflect the smaller number of sawtooth events ($\sim$100) compared to quiescent ensembles and the lower signal to noise level existing during a crash.

C. QSH

Data presented in Figs. 7 and 9 included only multiple helicity (MH) intervals in which the largest tearing modes are comparable in amplitude. Quasi-single helicity (QSH) periods differ in that the amplitude of a single mode dominates the n-spectrum.[38] The width of the spectrum is customarily quantified by the parameter, $N_s=1/\Sigma_n(W_n/\Sigma_{n'}W_{n'})^2$, where W_n is the energy of the $m=1$, n mode. A spectrum with only one mode corresponds to $N_s=1$. MH plasmas are defined to be periods where on average $N_s \geq 2$ while QSH is characterized by $N_s<2$. During QSH plasma periods in MST, the peak power of the $n=6$ poloidal magnetic field measured at the wall increases more than threefold whilst the power in other modes remains identical to the MH ensemble or drops slightly. A QSH ensemble of 0.5 ms intervals at each measurement location was selected from the same plasma discharges used for the MH ensembles; yet, higher baseline levels are present in the QSH ensembles due to the smaller number of QSH events ($\sim$200 to 300 intervals). Measurements during QSH periods (Fig. 10) show the dominant $m=1$, $n=6$ flow profile is clearly broadened in radius. Significant $n=6$ flow appearing well above the baseline at two measurement locations establishes the radial extent of the correlated flow to be greater than 9 cm but less than 27 cm. It is likely that the broadening of the $n=6$ tearing mode flow profile is a result of the increased magnetic island width in conjunction with the growth of the mode magnetic amplitude observed during QSH.[38]

Previous line-integrated spectroscopic measurements of tearing mode flows during QSH periods in MST suggested that an ordered helical flow pattern emerges when the plasma approaches a helical state.[38,39] Flows correlated with the $n=6$ mode were observed across most of the plasma radius. The localized flows illustrated in Fig. 10 are greater than the line-integrated measurements by at least a factor of two with measurement baselines larger than the line-integrated profiles, suggesting the two measurements could be consistent. Finally, local flows associated with the $n=7$ to 12 tearing modes during QSH are relatively unchanged in amplitude from the MH case while previous line-integrated flows indicate a small drop in these modes. Differences between the local and line-integrated flow magnitudes are likely due to spatial averaging of the line-integrated spectroscopic view across the plasma.

For comparison, line-integrated profiles of the recent spectroscopic measurements provided by the second background view (data not shown) reproduce several of the characteristics previously reported during QSH events. Common features include an increase of the $n=6$ tearing mode flow along with broader flow structures for all modes when compared to MH periods. Still, line-integrated peak flows remain significantly less than the peak localized flows, confirming that measurement localization is essential for determining the true amplitude and spatial extent of the tearing mode flows during QSH.

We conclude that while poloidal flows associated with the $n=6$ mode during QSH intervals are larger and broader, they do not dominate the flow spectrum over the entire radius in contrast to the magnetic spectrum. The $n=7$ to 12 modes maintain a similar flow structure during QSH while all tearing mode flows remain peaked near their resonant surfaces. The absence of any significant flow at the center of the plasma is not in agreement with single-fluid MHD models predicting a broadly peaked poloidal velocity fluctuation profile with the strongest flows on-axis.[39]

IV. MHD DYNAMO

The presence of tearing mode flows has a number of potential consequences including dynamo action, viscous ion heating, and particle, momentum, and energy transport. Dynamo action is predicted and observed in many plasma laboratory experiments including the reversed-field pinch[7,9,11] and the spheromak.[12,40,41] Dynamos are also believed to play a critical role in the dynamics of many natural geophysical and astrophysical systems such as the molten core of the Earth,[42] the sun, galaxies, accretion disks, and astrophysical jets.[43,44] We consider the role of the MHD dynamo, $\langle \tilde{\mathbf{v}} \times \tilde{\mathbf{b}} \rangle$ in MST as a result of measured tearing mode flows. The total MHD dynamo on the magnetic axis is established for the same plasma experiments reported in Sec. III and compared to expectations of the electric field and current profile from

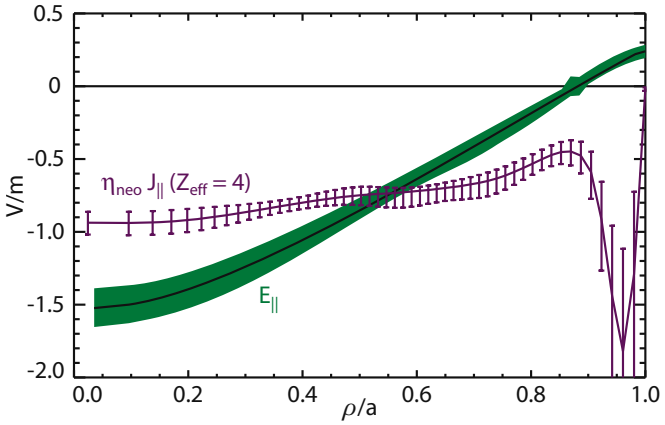

FIG. 11. (Color online) The parallel electric field and current profiles established by equilibrium reconstruction during quiescent periods. The total measured MHD dynamo on-axis is $+0.52 \pm 0.10$ V/m.

equilibrium reconstruction. Additionally, contributions to the total MHD dynamo resulting from poloidal tearing mode flows off-axis are calculated for the same assortment of plasma conditions.

In the RFP, dynamo action does not generate additional magnetic energy from kinetic energy or sustain magnetic energy for longer than resistive timescales. Instead, the RFP dynamo redistributes the magnetic profile by driving current in one region and suppressing it in another. Specifically, the dynamo works to flatten the peaked parallel (magnetic field aligned) current profile by increasing current in the edge of the plasma while reducing current in the core.[9–11,45] Figure 11 illustrates the flat parallel current profile relative to the core peaked applied electric field. The positive toroidal direction is defined as the direction of the mean magnetic field on-axis, yielding an electric field and current in the negative toroidal direction on-axis in MST. The difference between the applied parallel electric field and the resulting parallel current profile has long been presumed to be balanced by dynamo action.

In MST, the total magnetic energy far exceeds the total kinetic energy of the plasma. As a result the $\mathbf{J}\times\mathbf{B}$ back reaction of the magnetic field on the plasma flow is significant enough to strongly couple the magnetic field and the plasma flow. A strong field system is described by the generalized Ohm's law,

$$-\frac{m_e}{e^2 n_e}\frac{\partial \mathbf{J}}{\partial t}+\mathbf{E}+\mathbf{v}\times\mathbf{B}-\frac{1}{en_e}\mathbf{J}\times\mathbf{B}+\frac{\nabla P_e}{en_e}=\eta\mathbf{J}, \tag{3}$$

where m_e, e, n_e, and P_e are the electron mass, charge, density and pressure respectively. Writing each quantity as the sum of a mean and fluctuating component, while taking the flux surface average in toroidal geometry (average over poloidal and toroidal angle) reduces the parallel component to[7]

$$\eta\mathbf{J}_{\|}-\mathbf{E}_{\|}=\langle\tilde{\mathbf{v}}\times\tilde{\mathbf{b}}\rangle_{\|}-\frac{1}{en_e}\langle\tilde{\mathbf{j}}\times\tilde{\mathbf{b}}\rangle_{\|}, \tag{4}$$

where $\langle\ \rangle$ denotes a flux surface average. Parallel fluctuations in the pressure and current have been neglected in this analysis. The difference between the mean parallel electric field and the current profile is accounted for by fluctuations in the magnetic field correlated with either the velocity (single-fluid MHD dynamo) or current fluctuations (two-fluid Hall dynamo). Both dynamo terms have the potential to drive current along magnetic field lines and ultimately balance parallel Ohm's law. It is not yet fully understood where in the plasma and at what times during the sawtooth cycle each of the two dynamo terms contributes to satisfy parallel Ohm's law in the core of MST.

The importance of the two-fluid Hall dynamo has previously been investigated in the core of MST.[13] During a sawtooth crash, the Hall dynamo due to the $n=6$ dominant tearing mode is found to generate a large electromotive force that is localized to an ~8 cm radial width about the mode resonance surface. However, the parallel electric field during a sawtooth crash is measured to be large throughout the plasma volume and it is therefore anticipated the MHD dynamo will contribute significantly on the magnetic axis. Likewise, during quiescent plasma periods the Hall dynamo is small and is not expected to contribute to the parallel current at radii away from mode resonant surfaces such as near the magnetic axis.

Our technique for measuring the MHD dynamo is a mean field approach via averaging over flux surfaces and considering only the component parallel to the mean magnetic field. In MST, the mean magnetic field on-axis is completely in the toroidal direction; therefore, the parallel dynamo on-axis can only result from fluctuations perpendicular to the toroidal direction. Furthermore, at the origin the concept of a poloidal coordinate breaks down and the total MHD dynamo reduces to

$$\langle\tilde{\mathbf{v}}\times\tilde{\mathbf{b}}\rangle_{\|}=|\tilde{v}_{\perp}||\tilde{b}_{\perp}|\gamma_{vb}\cos\delta_{vb}, \tag{5}$$

where the MHD dynamo depends on the absolute magnitude of the perpendicular fluctuating velocity and magnetic field components, along with the coherence (γ) and the cosine of the phase difference between the velocity and magnetic signals (δ). The tearing mode magnetic fields are measured by an array of coils at the wall. Using the amplitude and phase of each magnetic mode, the magnetic field at the CHERS measurement location is calculated. The subsequent magnetic field corresponds to the component of $\tilde{b}_{\perp}$ along the diagnostic neutral beam path and perpendicular to the measurement of the tearing mode flows (see Fig. 1). Therefore, a measured phase difference of zero corresponds to prefect temporal phasing of $\tilde{v}_{\perp}$ and $\tilde{b}_{\perp}$ directed orthogonally to each other. For maximum MHD dynamo action to occur, the perpendicular velocity and magnetic fluctuations must be perfectly coherent with a phase difference of zero or π. A measured phase of zero generates MHD dynamo in the positive toroidal direction while a phase of π produces MHD dynamo in the negative toroidal direction. A phase other than zero or π indicates the $\tilde{v}_{\perp}$ and $\tilde{b}_{\perp}$ helical structures are shifted relative to one another and not quite optimal for producing maximum dynamo. Likewise, zero coherence or a phase difference of $\frac{\pi}{2}$ or $3\pi/2$ will result in zero MHD dynamo. It is assumed that $\tilde{v}_{\perp}$ and $\tilde{b}_{\perp}$ are circularly polarized on the magnetic axis.

To establish the total perpendicular tearing mode flow we reconstruct the total perpendicular magnetic fluctuation on-axis, at any given point in time, from the measured poloidal magnetic field fluctuations at the wall. To this end, an additional signal representing the combined magnetic fluctuations from all significant tearing modes on-axis was created and is denoted by "$\tilde{b}_{\mathrm{sum}}$". The $\tilde{b}_{\mathrm{sum}}$ signal is assembled before ensemble averaging by summing the time varying poloidal magnetic amplitudes associated with each $m=1$, $n=5$ to 12 tearing mode measured at the wall for each realization in the ensemble

$$\tilde{b}_{\mathrm{sum}}(t) \equiv \sum_{n=5}^{12} \tilde{b}_{\theta,n}(t). \tag{6}$$

The $\tilde{b}_{\mathrm{sum}}$ signal is carried through the ensemble averaging analysis in the same manner as the individual tearing modes. Due to the relative amplitudes of the core tearing modes (Fig. 5), $\tilde{b}_{\mathrm{sum}}$ is heavily weighted toward the largest amplitude modes with low n number. The correlated velocity baseline associated with $\tilde{b}_{\mathrm{sum}}$ is similar to the individual tearing mode baselines; however, the total fluctuating velocity from all modes combined is larger than for any given mode and hence can more easily be measured. Most importantly, correlation with the $\tilde{b}_{\mathrm{sum}}$ signal represents the most direct measure of the total MHD dynamo in the core of MST because it resolves the combined activity of all tearing modes.

A second method for determining the total MHD dynamo uses the magnetic and velocity fluctuations from individual modes, potentially yielding additional information about the contribution of each mode. Yet, velocity fluctuations near the magnetic axis for all the plasma regimes presented exhibit little or no significant correlation with any of the individual $m=1$ magnetic modes because the measured tearing mode flows are frequently comparable to the baselines. Therefore, contributions from the individual tearing modes suggest a weak MHD dynamo on-axis. The real correlated velocity fluctuations on the magnetic axis are possibly as large as the baseline for each mode but cannot be resolved with the current data.

The baseline for the MHD dynamo measurement can be calculated using the experimental constraints. The MHD dynamo baseline is computed assuming maximum coherence ($\gamma=\gamma^{\mathrm{baseline}}$) and perfect phasing between the velocity and magnetic fluctuations ($\delta=0,\pi$)

$$\langle \tilde{\mathbf{v}} \times \tilde{\mathbf{b}} \rangle_{\mathrm{baseline}} = |\tilde{v}_{\perp}||\tilde{b}_{\perp}|\gamma_{vb}^{\mathrm{baseline}}, \tag{7}$$

where $\gamma^{\mathrm{baseline}}$ is defined in Eq. (2). The baseline of the MHD dynamo is an unsigned quantity that represents the absolute bound (positive or negative) of the MHD dynamo for the case that correlated velocity fluctuations do not exist. Once a dynamo measurement has been resolved above the baseline a statistical analysis is performed to determine the uncertainty in the correlated product.

A. On-axis

The MHD dynamo measured on-axis during quiescent periods for each of the core tearing modes along with the corresponding baselines are calculated according to Eqs. (5) and (7). For each tearing mode the measured MHD dynamo on-axis is smaller or equal to its baseline, which is consistent with the tearing mode flows in Fig. 7 being similar to baseline. Nevertheless, there may still exist a finite positive MHD dynamo near the magnetic axis that cannot be resolved into individual modes using the current data. The total MHD dynamo calculated directly from the $\tilde{b}_{\mathrm{sum}}$ signal yields +0.52 V/m, larger than the $\tilde{b}_{\mathrm{sum}}$ baseline of 0.42 V/m. While the magnitude of the total MHD dynamo is not greatly above the baseline, we can conclusively state the real total MHD dynamo on-axis is greater than zero. Calculations of the MHD dynamo using random signals in place of the measured velocity fluctuations produce two common features. First, an equal proportion of positive and negative dynamo contributions are generated by the set of all tearing modes. Second, the calculation of the MHD dynamo contributions for each tearing mode is generally far below the MHD dynamo baseline. In contrast, each of the measured tearing mode contributions in the quiescent case has a positive contribution with magnitudes comparable to the baseline except for the $n=5$ mode, which is not always resonant. These two characteristics make it highly unlikely that the true MHD dynamo on-axis is zero. Finally, a statistical analysis establishes the uncertainty of the +0.52 V/m MHD dynamo measurement on-axis to be ± 0.10 V/m.

Comparing the $+0.52 \pm 0.10$ V/m measurement of the total parallel MHD dynamo on-axis to the difference between the parallel electric field and current profile in Fig. 11 can determine if the MHD dynamo is adequate to satisfy the parallel Ohm's law in MST. Equilibrium reconstruction using MSTFit[46] solves the Grad–Shafranov equation from measurements of the mean magnetic field at the edge of the plasma to determine the MHD equilibrium. The MSTFit calculations presented here also include line-integrated electron density measurements provided by interferometry as an input while assuming a neoclassical resistivity and $Z_{\mathrm{eff}}=4$. During quiescent periods, the MSTFit reconstruction reveals the magnitude and sign of the required dynamo action near the magnetic axis are consistent with the $+0.52 \pm 0.10$ V/m MHD dynamo measurement. Local measurements of the velocity fluctuations suggest the MHD dynamo is sufficient to satisfy parallel Ohm's law at the magnetic axis of the plasma during quiescent periods and contributions from other dynamo mechanisms are likely insignificant or cancel each other.

A similar analysis for the MHD dynamo on-axis is performed for sawtooth crash intervals. During a sawtooth crash, velocity fluctuations show modest correlation on-axis with the low n modes (Fig. 9). As a result, a finite MHD dynamo might be expected. The total MHD dynamo on the magnetic axis is computed for a time window of -0.3 to +0.1 ms relative to the sawtooth crash. Significant MHD dynamo action is observed, due mostly to the dominant $n=6$ tearing mode, resulting in a total dynamo of +6.6 V/m mea-

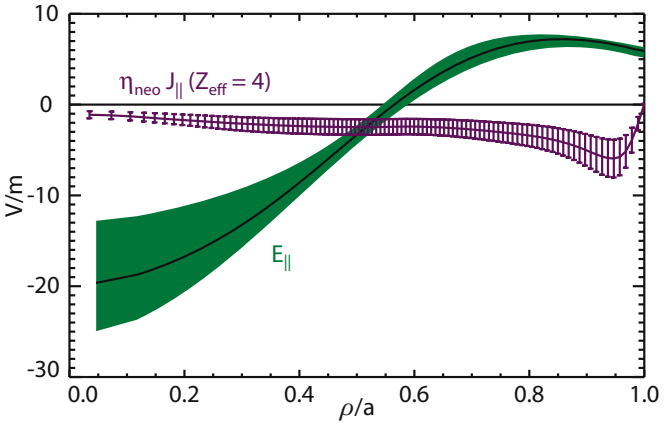

FIG. 12. (Color online) The parallel electric field and current profiles established by equilibrium reconstruction from −0.1 to +0.3 ms relative to a sawtooth crash. The total MHD dynamo on-axis measured from −0.3 to +0.1 ms relative to a sawtooth crash is +6.6 ± 1.1 V/m.

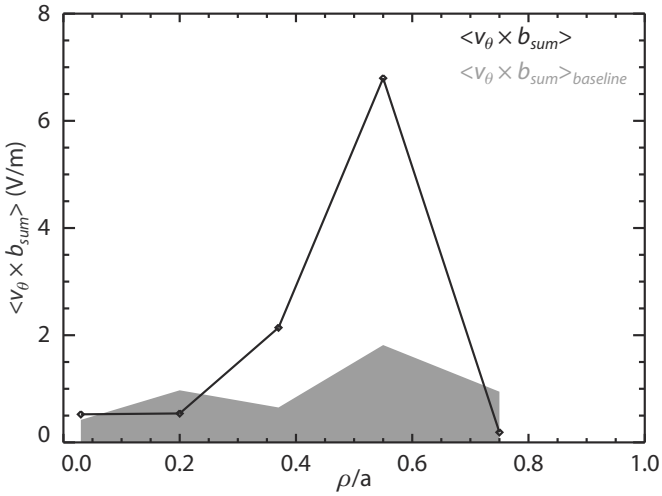

FIG. 13. Contributions to the MHD dynamo resulting from poloidal tearing mode flows during quiescent periods. The on-axis measurement represents the total MHD dynamo and the gray area indicates the $\tilde{b}_{sum}$ dynamo baseline at each measurement location.

surably above the baseline of 5.8 V/m. Higher n modes resonant away from the magnetic axis generate insignificant dynamo relative to their baselines. Again, while the measured $\tilde{b}_{sum}$ MHD dynamo is not far above the baseline, significant contributions from low n modes resonant near the magnetic axis imply the true total MHD dynamo during a crash is positive. Lastly, the uncertainty of the MHD dynamo measured during the crash is computed to be ±1.1 V/m.

Reconstruction of the parallel electric field and current profile during the crash shows the anticipated dynamo action on the magnetic axis is larger than the measured datum for $\tilde{b}_{sum}$ (Fig. 12). Error bars for the parallel electric field and current profile are determined by averaging over several sawtooth crashes. Vital to the accuracy of both the equilibrium reconstruction and the tearing mode correlation analysis is the need to average over finite time windows containing smooth signals with acceptable noise levels. The timing of the equilibrium reconstruction window relative to the sawtooth crash was chosen to achieve satisfactory fits to the electric field by selecting an interval over which the toroidal flux was increasing linearly. As a result, the equilibrium reconstruction was performed from −0.1 to +0.3 ms relative to the sawtooth crash, shifted later by 200 μs from the MHD dynamo measurements. Equilibrium reconstruction demonstrates a larger need for dynamo action following the crash than prior to it. Therefore, it is possible the difference in averaging windows between the equilibrium reconstruction and the measured dynamo might account for the discrepancy in dynamo action. On the other hand, the results may point to the need for an additional dynamo mechanism at the crash to balance parallel Ohm's law. The two-fluid Hall dynamo resulting from the $n=6$ tearing mode has been measured to be large at a sawtooth crash but localized to within ~8 cm of the resonant surface.[13] Likewise, it is possible the $n=5$ tearing mode resonant in the core after the crash could generate substantial Hall dynamo action near the magnetic axis.

In conclusion, measurements during the crash demonstrate that the MHD dynamo is significant but does not discount the contributions of other dynamo mechanisms. It is possible that the MHD dynamo becomes very large after the crash and is sufficient to account for the difference in the parallel current and electric field at all times. Alternatively, an additional dynamo mechanism could be active after the crash, but in either case the large dynamo action at the crash should decay on the order of milliseconds.

B. Off-axis

A complete measurement of the total parallel MHD dynamo at locations away from the magnetic axis requires all three components (r, θ, ϕ) of the velocity and magnetic field fluctuations. The measured tearing mode flows are limited to the poloidal component and hence give only one term of the toroidal dynamo by a cross product with the radial magnetic field fluctuations. We report on this *contribution* to the toroidal MHD dynamo generated by velocity fluctuations in the poloidal direction for the measured plasma regimes. It should be noted that the structure of the total parallel MHD dynamo off-axis could be very different from the measured contributions presented here, as the remaining three dynamo terms at any radial location could cancel or enhance the portion due to the poloidal velocity fluctuations.

Strong poloidal tearing mode flows at the plasma midradius during quiescent periods generate large MHD dynamo contributions, as shown in Fig. 13. The contributions to the toroidal dynamo produced by off-axis poloidal flows and radial magnetic fluctuations is more than an order of magnitude larger than the total MHD dynamo on-axis. Equilibrium reconstruction predicts a reversal of the total parallel dynamo action in MST from the core to the edge during both quiescent intervals and sawtooth crashes. Thus it is expected the addition of other MHD dynamo components or other dynamo mechanisms would reflect this sign change. A large toroidal dynamo in the edge due to the strong correlated poloidal flow fluctuations suggests the possibility of significant perpendicular $\langle \tilde{\mathbf{v}} \times \tilde{\mathbf{b}} \rangle$ that is excluded from the parallel dynamo analysis.

During a sawtooth crash, the total parallel dynamo is expected to be significant across the plasma radius due to the considerable correlated flow fluctuations highlighted in Fig. 9 and calculations yield substantial MHD dynamo activity. At a sawtooth crash, measurement noise and the limited number of events available for ensemble averaging drive the baselines above the measured dynamo at the outer two measurement locations (data not shown). Contributions to the MHD dynamo around the time of a sawtooth crash from correlated poloidal flows at the midradius are large when compared to the total dynamo action on the magnetic axis.

V. SUMMARY

Experiments described herein constitute the first local measurements of tearing mode flows in the core of a hot plasma. The measurements were made possible by the development of a novel duo spectrometer with concurrently high optical throughput and high dispersion optimized for high frequency measurements in MST laboratory plasmas. A modified Czerny–Turner layout is assembled with large optical components including two separate mosaic gratings capable of resolving low amplitude spectral emissions. Combining the innovative spectrometer with a hydrogen diagnostic neutral beam provides fast CHERS measurements of impurity ions in the plasma core localized to ~2 cm in the radial direction. Postprocessing of the raw spectroscopic emission accounts for asymmetries of the spectral line due to fine structure effects.

The flows generated by tearing modes play a fundamental role in the RFP dynamics. The recent diagnostic advances just described have enabled a study of the three-dimensional structure of tearing mode flows in the core of MST. Poloidal tearing mode flows are observed to be localized to the resonant surface with a radial extent on the order of the magnetic island width. These flows measurements are consistent with previous line-integrated measurements[10] suggesting similar localization of the flow, but the new direct measurements confirm this result. The tearing mode flows are narrow when compared to the magnetic mode profiles but much broader than linear MHD calculations, suggesting a number of possible nonlinear MHD or non-MHD effects are important to determining the radial breadth of the tearing mode flow. The amplitudes of the tearing mode flows are approximately three orders of magnitude less than the Alfvén velocity, in agreement with single-fluid MHD computation. However, the poloidal flow n-spectrum differs significantly from the magnetic n-spectrum. During quiescent intervals, the largest correlated flows of ~1.5 km/s are measured in association with modes having higher toroidal mode numbers, smaller magnetic amplitudes, and a resonance near the midradius. Dominant tearing modes characterized by lower toroidal mode numbers generate modest poloidal flow fluctuations of ~0.7 km/s closer to the magnetic axis. While the approximate magnitude of the predicted flow velocities are in agreement with the measurements, the trend with n number is not. At a sawtooth crash, characterized by a surge in the reconnection activity, correlated flow amplitudes increase substantially to ~3 to 4 km/s, become similar in magnitude for all tearing modes resonant in the core, and broaden in the radial direction. Results from QSH plasmas demonstrate a broadening of the $m=1$, $n=6$ flow structure consistent with an increase of the magnetic island width but still yielding flows near the resonant surface.

The tearing mode flows in MST are responsible for modification of the plasma equilibrium through dynamo action. Calculations of the MHD dynamo due to the presence of poloidal tearing mode flow profiles yield the complete MHD dynamo on-axis and contributions to the toroidal component off-axis. The total MHD dynamo on-axis is measured to be $+0.52 \pm 0.10$ V/m during quiescent periods and is sufficient to account for the discrepancy between the parallel electric field and the current. During a sawtooth crash the measured MHD dynamo on-axis is $+6.6 \pm 1.1$ V/m. While the measurement is significant when compared to the dynamo action needed to balance parallel Ohm's law, it does not exclude other dynamo mechanisms, such as the Hall dynamo, from contributing during intense reconnection activity. Contributions to the toroidal MHD dynamo resulting from large poloidal flows at the midradius generate considerable dynamo action during both quiescent intervals and sawtooth crashes in comparison to the total dynamo action on-axis. These calculations reflect the structure of the tearing mode flows, implying the phase between the velocity and magnetic fluctuations is favorable for dynamo action and robust across plasma regimes.

ACKNOWLEDGMENTS

Special thanks to the excellent scientific and technical staff at MST. In particular, the authors would like to thank W. X. Ding, T. Yates, J. A. Reusch, and D. J. Holly for their contributions. Work supported by the US DOE (Contract No. DE-FC02-05ER54814) and NSF (Contract No. PHY 0821899).

[1] H. P. Furth, J. Killeen, and M. N. Rosenbluth, Phys. Fluids **6**, 459 (1963).
[2] D. Biskamp, *Nonlinear Magnetohydrodynamics* (Cambridge University Press, Cambridge, 1997).
[3] P. H. Rutherford, Phys. Fluids **16**, 1903 (1973).
[4] R. Pellat, M. Frey, and M. Tagger, J. Phys. (Paris) **45**, 1615 (1984).
[5] S. Assadi, S. C. Prager, and K. L. Sidikman, Phys. Rev. Lett. **69**, 281 (1992).
[6] A. K. Hansen, A. F. Almagri, D. Craig, D. J. Den Hartog, C. C. Hegna, S. C. Prager, and J. S. Sarff, Phys. Rev. Lett. **85**, 3408 (2000).
[7] H. Ji, A. F. Almagri, S. C. Prager, and J. S. Sarff, Phys. Rev. Lett. **73**, 668 (1994).
[8] P. W. Fontana, D. J. Den Hartog, G. Fiksel, and S. C. Prager, Phys. Rev. Lett. **85**, 566 (2000).
[9] J. T. Chapman, Ph.D. thesis, University of Wisconsin-Madison, 1998.
[10] D. J. Den Hartog, J. T. Chapman, D. Craig, G. Fiksel, P. W. Fontana, S. C. Prager, and J. S. Sarff, Phys. Plasmas **6**, 1813 (1999).
[11] S. Ortolani and D. D. Schnack, *Magnetohydrodynamics of Plasma Relaxation* (World Scientific, Singapore, 1993).
[12] A. al-Karkhy, P. K. Browning, G. Cunningham, S. J. Gee, and M. G. Rusbridge, Phys. Rev. Lett. **70**, 1814 (1993).
[13] W. X. Ding, D. L. Brower, D. Craig, B. H. Deng, G. Fiksel, V. Mirnov, S. C. Prager, J. S. Sarff, and V. Svidzinski, Phys. Rev. Lett. **93**, 045002 (2004).
[14] R. C. Isler and L. E. Murray, Appl. Phys. Lett. **42**, 355 (1983).
[15] R. J. Fonck, R. J. Goldston, R. Kaita, and D. E. Post, Appl. Phys. Lett. **42**, 239 (1983).
[16] D. Craig, D. J. Den Hartog, G. Fiksel, V. I. Davydenko, and A. A. Ivanov, Rev. Sci. Instrum. **72**, 1008 (2001).

[17]D. J. Den Hartog, D. Craig, D. A. Ennis, G. Fiksel, S. Gangadhara, D. J. Holly, J. C. Reardon, V. I. Davydenko, A. A. Ivanov, A. A. Lizunov, M. G. O'Mullane, and H. P. Summers, Rev. Sci. Instrum. **77**, 10F122 (2006).
[18]H. T. Evensen, R. Durst, R. J. Fonck, and S. F. Paul, Rev. Sci. Instrum. **66**, 845 (1995).
[19]H. T. Evensen, R. J. Fonck, S. F. Paul, G. Rewoldt, S. D. Scott, W. M. Tang, and M. C. Zarnstorff, Nucl. Fusion **38**, 237 (1998).
[20]D. J. Den Hartog, A. F. Almagri, J. T. Chapman, H. Ji, S. C. Prager, J. S. Sarff, R. J. Fonck, and C. C. Hegna, Phys. Plasmas **2**, 2281 (1995).
[21]D. J. Den Hartog and D. Craig, Plasma Phys. Controlled Fusion **42**, L47 (2000).
[22]D. Craig, D. J. Den Hartog, D. A. Ennis, S. Gangadhara, and D. Holly, Rev. Sci. Instrum. **78**, 013103 (2007).
[23]S. Gangadhara, D. Craig, D. A. Ennis, and D. J. Den Hartog, Rev. Sci. Instrum. **77**, 10F109 (2006).
[24]H. P. Summers, The ADAS User Manual, 2.6 ed., ADAS, 2004, http://www.adas.ac.uk.
[25]R. J. La Haye, T. N. Carlstrom, R. R. Goforth, G. L. Jackson, M. J. Schaffer, T. Tamano, and P. L. Taylor, Phys. Fluids **27**, 2576 (1984).
[26]D. Brotherton-Ratcliffe, C. G. Gimblett, and I. H. Hutchinson, Plasma Phys. Controlled Fusion **29**, 161 (1987).
[27]V. Antoni and S. Ortolani, Plasma Phys. **25**, 799 (1983).
[28]I. H. Hutchinson, M. Malacarne, P. Noonan, and D. Brotherton-Ratcliffe, Nucl. Fusion **24**, 59 (1984).
[29]R. B. Howell, J. C. Ingraham, G. A. Wurden, P. G. Weber, and C. J. Buchenauer, Phys. Fluids **30**, 1828 (1987).
[30]W. Shen, R. N. Dexter, and S. C. Prager, Phys. Rev. Lett. **68**, 1319 (1992).
[31]P. R. Brunsell, Y. Yagi, Y. Hirano, Y. Maejima, and T. Shimada, Phys. Fluids B **5**, 885 (1993).
[32]S. Mazur, Phys. Plasmas **1**, 3356 (1994).
[33]W. X. Ding, D. L. Brower, S. D. Terry, D. Craig, S. C. Prager, J. S. Sarff, and J. C. Wright, Phys. Rev. Lett. **90**, 035002 (2003).
[34]D. D. Schnack, D. C. Barnes, Z. Mikic, D. S. Harned, and E. J. Caramana, J. Comput. Phys. **70**, 330 (1987).
[35]D. L. Brower, W. X. Ding, S. D. Terry, J. K. Anderson, T. M. Biewer, B. E. Chapman, D. Craig, C. B. Forest, S. C. Prager, and J. S. Sarff, Rev. Sci. Instrum. **74**, 1534 (2003).
[36]S. Hokin, A. Almagri, S. Assadi, J. Beckstead, G. Chartas, N. Crocker, M. Cudzinovic, D. Den Hartog, R. Dexter, D. Holly, S. Prager, T. Rempel, J. Sarff, E. Scime, W. Shen, C. Spragins, C. Sprott, G. Starr, M. Stoneking, C. Watts, and R. Nebel, Phys. Fluids B **3**, 2241 (1991).
[37]T. M. Biewer, C. B. Forest, J. K. Anderson, G. Fiksel, B. Hudson, S. C. Prager, J. S. Sarff, J. C. Wright, D. L. Brower, W. X. Ding, and S. D. Terry, Phys. Rev. Lett. **91**, 045004 (2003).
[38]P. Martin, L. Marrelli, G. Spizzo, P. Franz, P. Piovesan, I. Predebon, T. Bolzonella, S. Cappello, A. Cravotta, D. F. Escande, L. Frassinetti, S. Ortolani, R. Paccagnella, D. Terranova, the RFX team, B. E. Chapman, D. Craig, S. C. Prager, J. S. Sarff, the MST team, P. Brunsell, J.-A. Malmberg, J. Drake, the EXTRAP TR2 team, Y. Yagi, H. Koguchi, Y. Hirano, the TPE-RX team, R. B. White, C. Sovinec, C. Xiao, R. A. Nebel, and D. D. Schnack, Nucl. Fusion **43**, 1855 (2003).
[39]P. Piovesan, D. Craig, L. Marrelli, S. Cappello, and P. Martin, Phys. Rev. Lett. **93**, 235001 (2004).
[40]P. M. Bellan, *Spheromaks: A Practical Application of Magnetohydrodynamic Dynamos and Plasma Self-Organization* (Imperial College Press, London, 2000).
[41]C. R. Sovinec, J. M. Finn, and D. Del-Castillo-Negrete, Phys. Plasmas **8**, 475 (2001).
[42]H. K. Moffatt, *Magnetic Field Line Generation in Electrically Conducting Fluids* (Cambridge University Press, Cambridge, 1978).
[43]E. N. Parker, *Cosmical Magnetic Fields: Their Origin and Their Activity* (Clarendon, Oxford, 1979).
[44]G. Rüdiger and R. Hollerbach, *The Magnetic Universe: Geophysical and Astrophysical Dynamo Theory* (Wiley-VCH, Weinheim, 2004).
[45]J. K. Anderson, J. Adney, A. Almagri, A. Blair, D. L. Brower, M. Cengher, B. E. Chapman, S. Choi, D. Craig, D. R. Demers, D. J. Den Hartog, B. Deng, W. X. Ding, F. Ebrahimi, D. Ennis, G. Fiksel, C. B. Forest, P. Franz, J. Goetz, R. W. Harvey, D. Holly, B. Hudson, M. Kaufman, T. Lovell, L. Marrelli, P. Martin, K. McCollam, V. V. Mirnov, P. Nonn, R. O'Connell, S. Oliva, P. Piovesan, S. C. Prager, I. Predebon, J. S. Sarff, G. Spizzo, V. Svidzinski, M. Thomas, and M. D. Wyman, Phys. Plasmas **12**, 056118 (2005).
[46]J. K. Anderson, C. B. Forest, T. M. Biewer, J. S. Sarff, and J. C. Wright, Nucl. Fusion **44**, 162 (2004).